



Synthesis and Characterization of Fe₃O₄ and Au- co-doped Fe₃O₄

Mohammed Abd Alhussein and Ahmed N. Abd

Department of Chemistry – College of sciences – University of Diyala

scichems2130@uodiyala.edu.iq

Received: 25 July 2022

Accepted: 26 August 2022

DOI: <https://dx.doi.org/10.24237/ASJ.01.02.645B>

Abstract

Co-precipitation was used to synthesis Au/Fe₃O₄ nano-composites different Au contents, (XRD) , (SEM) were used to analyze the nano-composites' microstructure and phase (EDX) , (XPS) were used to confirm the compositions of the powders. UV-Vis spectroscopy utilized to examine the particles' band gaps. Malachite green(MG) degradation was examined using the photocatalytic property of the nanocomposites, also the powders with 0.5 mol of Au exhibit the highest photocatalytic degradation efficiency. The reaction conditions for Au(0.5)/Fe₃O₄ were also evaluated.

Keywords: Synthesis, Characterization, Fe₃O₄, Au-doped Fe₃O₄



تحضير وتشخيص اوكسيد الحديد واوكسيد الحديد المطعم بالذهب

محمد عبد الحسين سلومي واحمد نجم عبد

قسم علوم الكيمياء – كلية العلوم – جامعة ديالى

الخلاصة

تم استخدام طريقه الترسيب المشترك لتحضير متراكبات نانوية (اوكسيد الحديد واوكسيد الحديد المطعم بالذهب) وتم تشخيصهم بالتقنيات التالية حيث استخدمت تقنية التحليل الطيفي للأشعة فوق البنفسجة والمرئية لفحص فجوة نطاق الجسيمات واستخدمت تقنية المسح المجهرى للإلكترون وتقنية الأشعة السينية لتحليل البنية المجهرية وتم فحص نحل صبغه الملاكيث اخضر باستخدام خاصية التحفيز الضوئي للمركبات النانوية والمساحيق التي تحتوي على 0.5 مول من الذهب تظهر اعلى كفاءة تحفيز ضوئي وتم ايضا تقييم ظروف التفاعل للمتراكبات النانوية.

الكلمات المفتاحية: تحضير، تشخيص، اوكسيد الحديد، اوكسيد الحديد المطعم بالذهب.

Introduction

Magnetic-plasmonic materials have attracted a lot of attention recently due to their potential as bifunctional nanomaterials in a range of fields, including biomedicine, biolabelling, optics, electronics, and catalysis[1,2]. The magnetic component of magnetic-plasmonic materials is typically composed of superparamagnetic iron oxides nanoparticles (SPION), which are employed in the treatment of wastewater, heterogeneous catalysis, drug delivery, cancer treatment, magnetic resonance imaging (MRI), biological separation, photocatalysis, and hyperthermia [3,4]. And made of a noble metal like Au for the plasmonic component. its use in improved oxidation processes, biocompatible systems, antimicrobial materials, and electrochemical sensors (AOPs) [5,6]. AOPs have recently reported a high efficiency in wastewater treatment and pollutant degradation due to their stimulation of the production of highly reactive hydroxyl radicals with a significant oxidation potential [7, 9] Malachite green, Acid Orange 7, Basic Violet 10, Ciprofloxacin, Moxifloxacin, Arsenate, and Nitrophenol, among other AOPs, have been degraded via sonolysis, sonocatalysis, sonophotocatalysis,



electrocoagulation, electro-peroxene, and the Fenton process [8,11]. However, the characteristics of magnetic-plasmonic materials are significantly influenced by the form and particle size distribution [12]. In this context, the application of eco-friendly chemicals and the employment of physicochemical methods that reduce or totally eliminate the use of hazardous chemical reagents are essential for the implementation and development of novel technologies to synthesize magnetic plasmonic materials [13,15]. Sonochemistry has received a lot of attention in recent years since it has a wide range of applications in numerous scientific domains. However, there hasn't been much research done on the possible uses of sonochemistry[13,14]. The dispersion of reactive species during the synthesis process is improved by the use of ultrasound in chemical processes, specifically in the sonochemical synthesis of nanomaterials. The acoustic cavitation phenomenon is caused by the propagation of ultrasonic waves in a liquid, which destroys the attraction interactions between molecules in the liquid phase. This event gives the reaction a mechanical activation. [1]. Typically, the sonochemical synthesis is used to create well-dispersed, core-shell nanoparticles [1]. The use of ultrasound in chemical processes, namely in the sonochemical synthesis of nanomaterials, enhances the dispersion of reactive species during the synthesis process. The destruction of the molecules' attractive forces in the liquid phase results from the propagation of ultrasonic waves in a liquid, which causes the acoustic cavitation phenomenon. This phenomenon provides an activation mechanism for the reaction. The use of green chemistry, on the other hand, has played a significant role in the synthesis of metallic and bimetallic nanoparticles since it reduces or eliminates the usage and/or creation of hazardous compounds[5,16,17]. Given that these organic components are directly involved in the reduction of metallic ions, the abundance of organic and biocompatible components present in plant extracts (such as antioxidants, phenolic compounds, flavonoids, which include flavones, flavanols, isoflavones, flavanones, and anthocyanidins) has encouraged the use of plant extracts as reducing or stabilizing agents in the synthesis of nanomaterials [18,19]. It has been reported that endemic plant species like *Cynara cardunculus*, *Silybum marianum*, *Lonicera japonica*, *Melissa officinalis*, *Artemisia absinthium*, *Anthemis nobilis*, *Lonicera japonica*, *Thymus kotschyianus*, *Moringa oleifera* flower, *Cnicus Benedictus*, and *Justicia spica* have been used to produce gold and iron oxide nanoparticles NP



[20,21]however, the Piper auritum extract has not been used to create magnetic plasmonic nanoparticles with the composition Au/Fe₃O₄. In the tropical region of Central America, there is an endemic plant called Piper auritum, which has medicinal properties. Due to the abundance of phytoalexins, which are low molecular weight compounds produced by biotic and abiotic stressors in the Piper auritum, these plants have antibacterial capabilities [22,23]. In this regard, our work suggests the environmentally friendly synthesis of Au/Fe₃O₄ nanoparticles using sonochemical activation and Piper auritum extract. Au/Fe₃O₄ nanoparticles with significant catalytic and magnetic properties can be obtained using a practical technology thanks to the synergistic effect of green and sonochemical synthesis.

Experimental

Materials

No	Substance	Chemical Formula	Purity%	Suppliers
1	Ferric nitrate	Fe(NO ₃) ₃ .9H ₂ O	98.0	THOMAS BAKER
2	Sodium citrate	Na ₃ C ₆ H ₅ O ₇	99.9	HIMEDIA
3	Ammonia	NH ₃ solution	99.7	CDH
4	Sodium hydroxide	NaOH solution	99	BDH
5	deionized water	H ₂ O	99	Lab
6	Ethanol absolute	C ₂ H ₅ OH	99.9	Merck
7	Hydrogen tetrachloroaurate trihydrate	HAuCl ₄ .3H ₂ O	99.9	ABCR

Au/Fe₃O₄ nanoparticles synthesis.

One and two mM HAuCl₄.3H₂O were mixed separately with 0.1g of ferric oxide in two 100ml beakers. Then 3ml of 1M sodium citrate solution was added at room temperature, and the temperature was raised to 80°C until the solution turned purple. It was then filtered and rinsed in 50ml of ethanol, acetone, and distilled water respectively and dried for three hours at 70°C.

Fe₃O₄ nanoparticles synthesis

In 250mL glass beaker, 1g of ferric nitrate nonahydrate Fe(NO₃)₃.9H₂O was mixed with 50 ml deionized water to make Fe₃O₄ NPs. After 2 hours, After 2 hours at room temperature the OH drop by drop 4NHreaction mixture was quenched with aqueous until the solution became a dark

brown precipitate. The powder was stored in the oven for 24 hours before being calcined at 400oC for 4 hours to produce nanoparticles [24].

Results and Discussion

Scanning electron microscopy (SEM)

Figure (1) (A) Shows the (SEM) of Fe₃O₄ with magnification strengths of 500 nm. It appears that Fe₃O₄ has an irregular form, with different particle sizes. Clusters of nanoparticles are observed. Figure (1) (B) Shows the scanning electron microscopy images of (0.8mM) Au-doped Fe₃O₄ nano oxide with a 500 nm magnification force. This explains that (0.8mM) Au-doped Fe₃O₄ nano oxide was composed of irregularly shaped nanoparticles. Surface of Au-doped (0.8mM) Fe₃O₄ is porous, contains pores, and is rough. Figure (1) (C) Shows the scanning electron microscopy pictures of (1.6mM) Au-doped Fe₃O₄ nano oxide with a magnification force of 500 nm. The image reveals that the shape of the particles is heterogeneous and irregular, as their surface is porous.

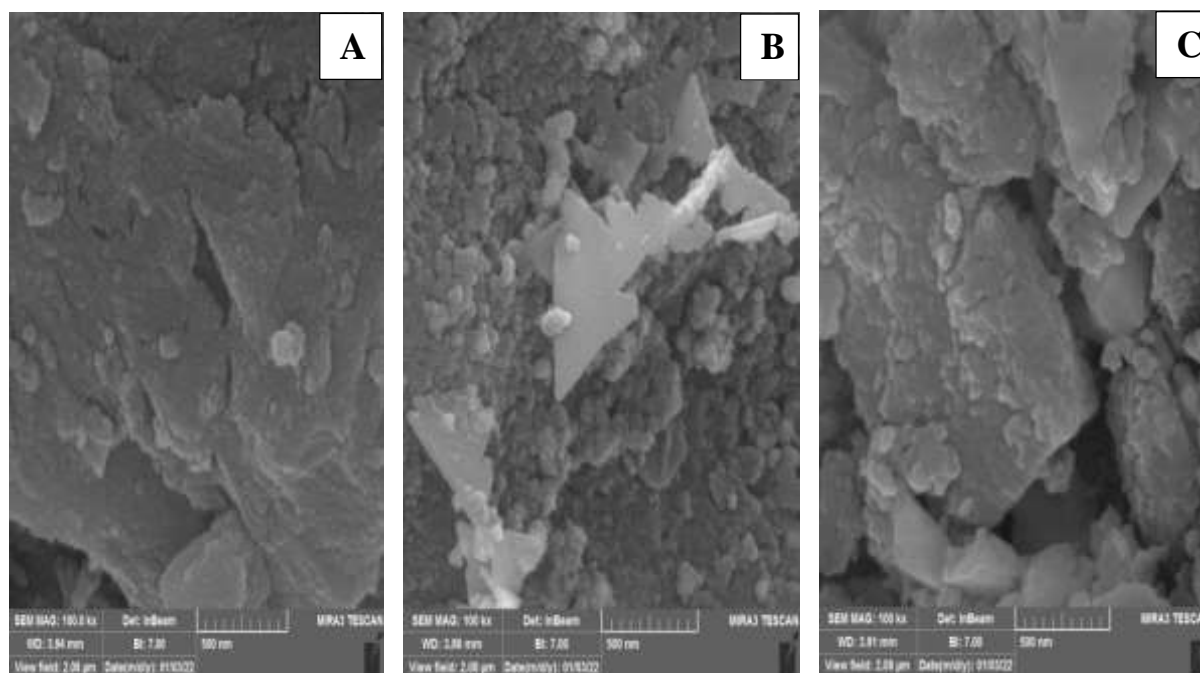


Figure1 : (A) Fe₃O₄, (B) (0.8mM) Au-dopedFe₃O₄ and (C) (1.6mM)Au-dopedFe₃O₄



X-Ray diffraction analysis

Figure (2) (A) Based on a comparison of the sample's XRD patterns with the typical patterns of cubic phase-structured Fe₃O₄ (JCPDS 00-019-0629), the XRD results demonstrate the formation of Fe₃O₄. The diffraction peaks (311) (34.5), (533) (74.2), (400) (43.12), (440) (62.54), (511) (57.88), (220) (32.33), and (111) (17.55) are essentially equal to the distinctive peaks of the Fe₃O₄ crystal. The ferric nano oxide's estimated particle size is 11.64 nm. Sharp peaks in XRD samples and particles smaller than 100 nm indicate that the surface is nanocrystalline.

Figure (2) (B) Based on a comparison of the sample's XRD patterns with the standard patterns of (0.8mM) Au-doped Fe₃O₄ (Fe₃O₄ JCPDS 00-019-0629) and (Au JCPDS 00-004-0784) of cubic phase structure, the XRD results demonstrate the development of (0.8mM) Au-doped Fe₃O₄. The diffraction peaks corresponding to (311) (35.1), (400) (43.55), (533) (74.11), (220) (29.55), and (440) (62.33) and doped Au to (111) (38.33), (200) (44.11), and (220) (64.43) are very similar to the peaks that are characteristic of the Au/Fe₃O₄ crystal. The particle size of the Au-doped Fe₃O₄ nano oxide (0.8mM) is estimated to be 17 nm. The presence of strong peaks in XRD samples and a particle size of less than 100 nm indicates that the surface is nanocrystalline.

Figure (2) (C) According to the sample's XRD, (1.6 mM) Au-doped Fe₃O₄ was formed. based on a comparison of their XRD patterns with the standard patterns of (1.6mM) Au-doped Fe₃O₄, (Fe₃O₄ JCPDS 00-019-0629) and (Au JCPDS (00-004-0784) of cubic phase structure, it has been determined that their phase structure is cubic. The diffraction peaks corresponding to (311) (35.77), (400) (43.55), (533) (74.5), (511) (57.77), (422) (53.7), (220) (30.5), (111) (20.1), and (440) (63.45), doped (Au) to (111) (43.77), (200) (44.2), and (220) (64.3) are very equivalent to the typical peaks of the Au-doped Fe₃O₄ crystal (1.6 mM). The (1.6 mM) Au-doped Fe₃O₄ nano oxide's estimated particle size is 21 nm. The nanocrystalline structure of the surface is indicated by the appearance of strong peaks in XRD samples and particle sizes less than (100) nm.

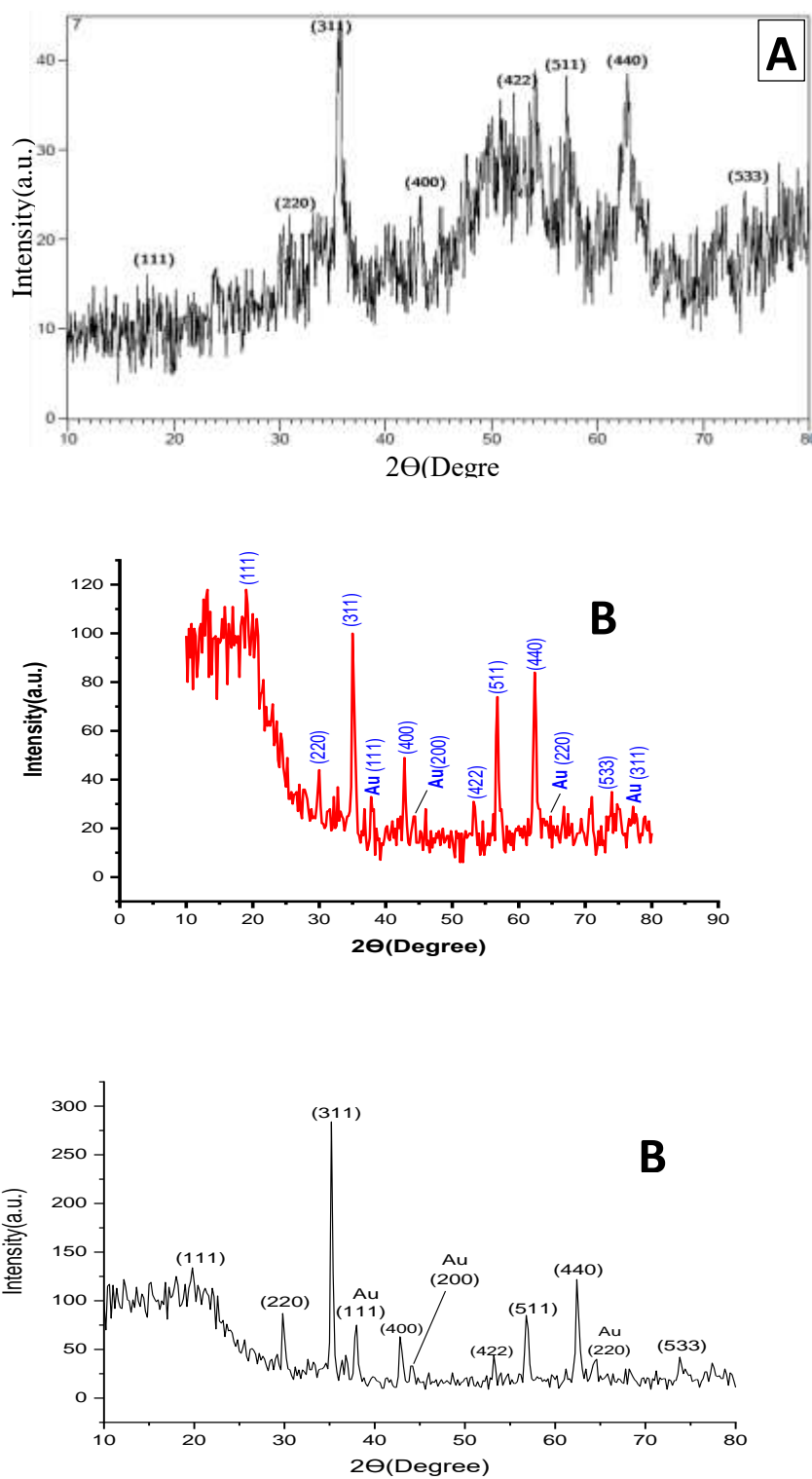


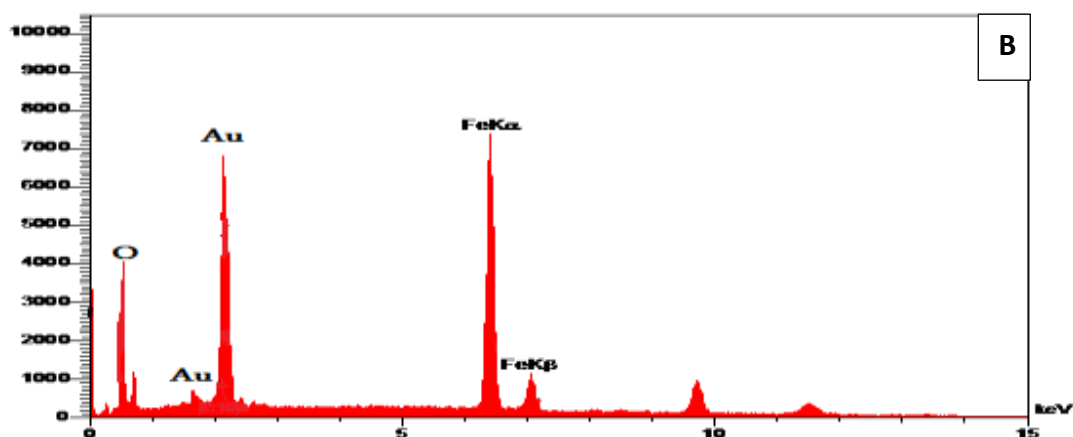
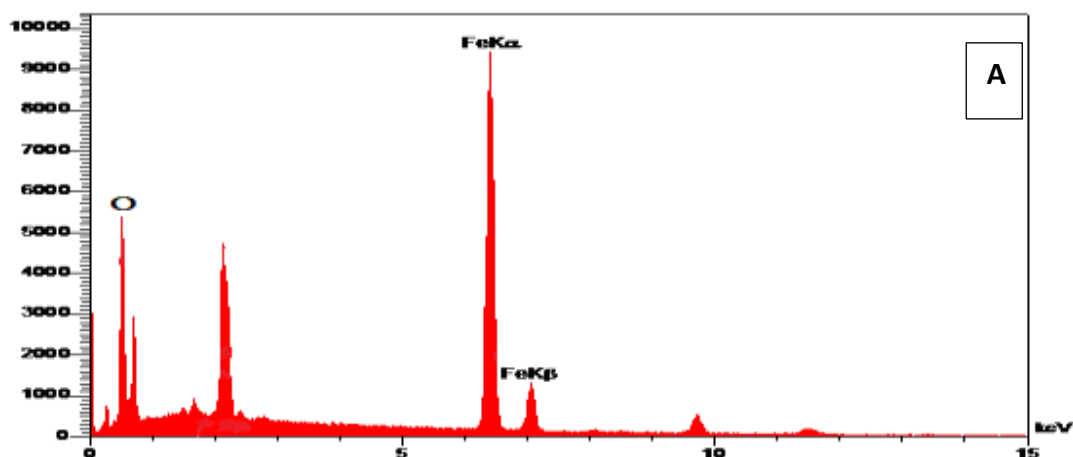
Figure 2: (A) Fe_3O_4 , (B) (0.8mM) Au-doped Fe_3O_4 and (C) (1.6mM) Au-doped Fe_3O_4

Table 1 :XRD Parameter associated to the nanoparticles.

Sample	2 θ	d-spacing	FWHM	Size
Fe ₃ O ₄	35.6329	2.51757	0.7200	11.64
Au/Fe ₃ O ₄ (0.8mM)	35.098	2.5547	0.491	17
Au/Fe ₃ O ₄ (1.6mM)	35.305	2.5401	0.399	21

Energy Dispersive X-ray Analysis (EDXA)

The EDXA is used to represents the presence of elements and their percentage in nature. Figure (3) (A, B, and C). Show the EDXA result of Fe₃O₄ and Au-doped Fe₃O₄ nanoparticles.



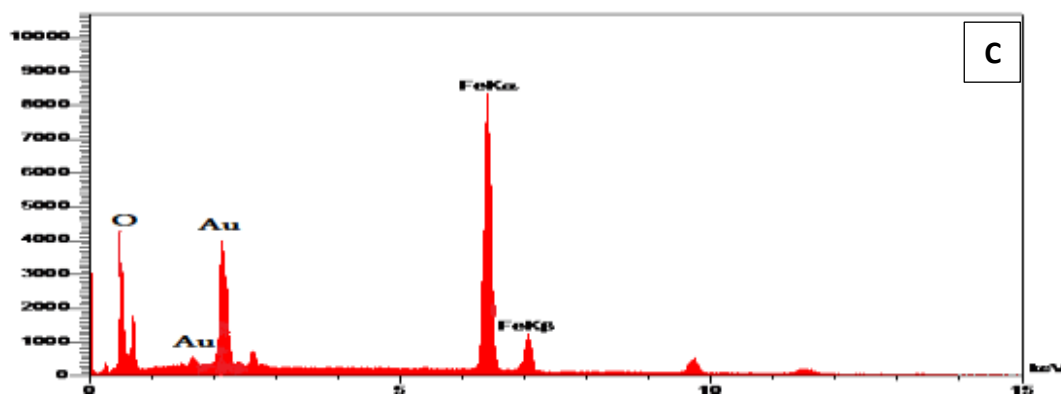
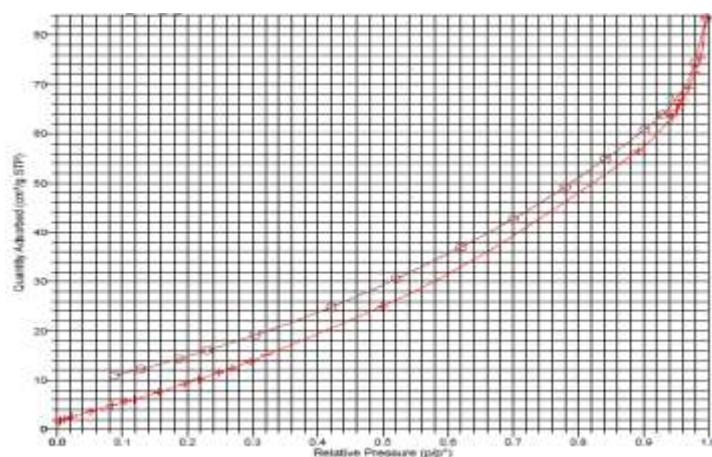


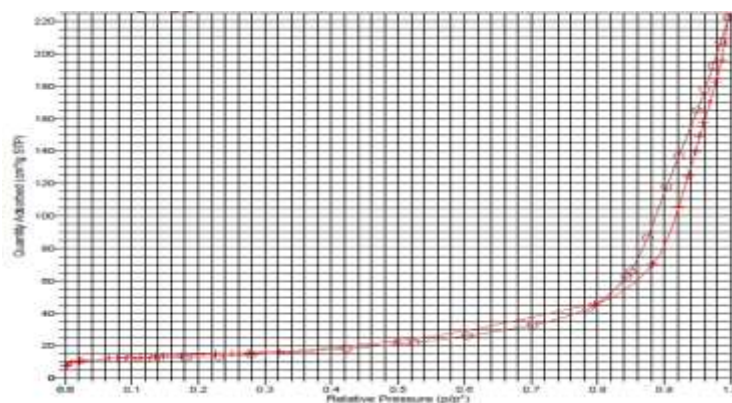
Figure 3: (A) Fe_3O_4 , (B) (0.8mM) Au-doped Fe_3O_4 and (C) (1.6mM) Au-doped Fe_3O_4 .

Porosity and surface area analysis

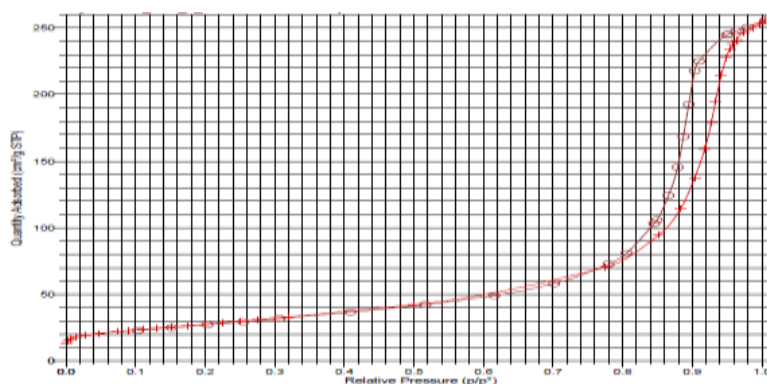
The pore size and surface area of the (Fe_3O_4 , Au-doped Fe_3O_4) were measured using the Brunauer-Emmett-Teller (BET) nitrogen adsorption methodology. These pore size data reveal the meso porosity of the neat and doped powders. Additionally, the adsorption-desorption isotherm plots that result in the surface area of nanoparticles are shown in the insets of Figure (4) (A, B and C). The effects of precious metals doping on the pore size and surface area of the prepared nano powder were also evident in figures (A, B and C). Particularly when Au was present, the surface areas dropped while the pore sizes increased the porous structure could provide enough of active sites and adequate mass transfer resistance for the degrading reaction.



(A)



(B)



(C)

Figure 4: (A) Fe_3O_4 , (B) (0.8mM) Au-doped Fe_3O_4 and (C) (1.6mM) Au-doped Fe_3O_4 .

Table (4-2): The values Surface area and porosity of prepared nanoparticles.

Sample	Surface Area	Pore volume	Pore diameter D_v/d
Fe_3O_4	11.7646	0.129264	35.37662
$\text{Fe}_3\text{O}_4(0.8\text{mM})$	38.5963	0.223393	26.58866
$\text{Fe}_3\text{O}_4(1.6\text{mM})$	74.6045	0.355500	20.35234

Conclusion

In conclusion, the co-precipitation method was used to prepare Au coated Fe_3O_4 nanoparticles, and different techniques XRD, EDXA, SEM. BET were used to examine the structure, functional groups, morphology, and magnetization properties. It was discovered that the average crystallite size and physical size of the produced nanoparticles decreased with



increasing weight of Au and the Oxides were used to removal organic pollutants from aqueous solution.

Acknowledgement

The authors express their sincere thanks and gratitude to the Department of chemistry, College of sciences University of Diyala, Iraq for providing the facilities for all laboratory tests.

References

1. N. J. Vickers, *Current biology*, 27(14), 713-715(2017)
2. F. H. Lin, R. A. Doong, *The Journal of Physical Chemistry C*, 121(14),7844-7853(2017)
3. A. Thamilselvan, P. Manivel, V. Rajagopal, N. Nesakumar, V. Suryanarayanan, *Colloids and Surfaces B: Biointerfaces*, 180, 1-8(2019)
4. N. J. Vickers, *Current biology*, 27(14), 713-715(2017)
5. C. Vijilvani, M. R. Bindhu, F. C. Frincy, M. S. AlSalhi, S. Sabitha, K. Saravanakumar, M. Atif, *Journal of Photochemistry and Photobiology B: Biology*, 202,111713(2020)
6. P. Eghbali, A. Hassani, B. Sündü, Ö. Metin, *Journal of Molecular Liquids*, 290,111208(2019)
7. F. Ghanbari, F. Zirrahi, K. Y. A. Lin, B. Kakavandi, A. Hassani, *Journal of Environmental Chemical Engineering*, 8(5), 104167(2020)
8. S. J. Crase, C. Hockaday, P. C. McCarville, *Journal of Adolescence*, 30(3),505-512(2007)
9. A. Khataee, T. S. Rad, S. Nikzat, A. Hassani, M. H. Aslan, M. Kobya, E. Demirbaş, *Chemical Engineering Journal*, 375, 122102(2019)
10. B. Jain, A. Hashmi, S. Sanwaria, A. K. Singh, M. A. B. H. Susan, S. A. Carabineiro, *Analytical Chemistry Letters*, 10(1),21-32(2020)
11. E. C.Lumbaque, E. R. L. Tiburtius, M. Barreto-Rodrigues, C. Sirtori, *Trends in Environmental Analytical Chemistry*, 24, e00069(2019)
12. F. Roy, A. E. Taouil, F. Lallemand, O. Heintz, V. Moutarlier, J. Y. Hihn, *Ultrasonics sonochemistry*, 40,9-16(2018)
13. F. Z. Thari, H. Tachallait, N. E. El Alaoui, A. Talha, S. Arshad, E. Álvarez, Bougrin, *Ultrasonics sonochemistry*, 68,105222(2020)
14. M. S. Elshikh, T. W. Chen, G. Mani, S. M. Chen, P. J. Huang, M. A. Ali, A. M. Al-Mohaimed, *Ultrasonics sonochemistry*, 70, 105305(2021)
15. M. S. Samuel, S. Jose, E. Selvarajan, T. Mathimani, A. Pugazhendhi, *Journal of Photochemistry and Photobiology B: Biology*, 202, 111642(2020)
16. B. Khodadadi, M. Bordbar, M. Nasrollahzadeh, *Journal of colloid and interface science*, 493, 85-93(2017)



17. S. Qasim, A. Zafar, M. S. Saif, Z. Ali, M. Nazar, M. Waqas, M. Hasan, Journal of Photochemistry and Photobiology B: Biology, 204, 111784(2020)
18. A. de Jesus Ruiz-Baltazar, Inorganic Chemistry Communications, 120,p. 108158(2020)
19. Á. de Jesús Ruíz-Baltazar, Inorganic Chemistry Communications, 120,p. 108148(2020)
20. Á. de Jesús Ruíz-Baltazar, S. Y. Reyes-López, M. de Lourdes Mondragón-Sánchez, M. Estevez, A. R. Hernández-Martinez, R. Pérez, Results in Physics, 11, 1142-1149(2018)
21. M. M. M. Binds, M. H. M. Reis, V. L. Cardoso, D. C. Boffito, Ultrasonics sonochemistry, 51,pp. 111-119(2019)
22. L. A. Conde-Hernández, J. Á. Guerrero-Beltrán, Food chemistry, 142, 455-460(2014)
23. E. Aguilar-Urquizo, M. F. Itza-Ortiz, J. R. Sangines-Garcia, A. T. Pineiro-Vázquez, A. Reyes-Ramirez, B. Pinacho-Santana, Brazilian Journal of Poultry Science, 22, (2020)
24. Y.mWei, B. Han, X. Hu, Y. Lin, X. Wang, X. Deng, Procedia Engineering, 27, 632-637(2012)